



Ship-borne wind
profiling with lidar

P. Achtert et al.

This discussion paper is/has been under review for the journal Atmospheric Measurement Techniques (AMT). Please refer to the corresponding final paper in AMT if available.

Measurement of wind profiles by motion-stabilised ship-borne Doppler lidar

P. Achtert¹, I. M. Brooks¹, B. J. Brooks², B. I. Moat³, J. Prytherch¹,
P. O. G. Persson⁴, and M. Tjernström⁵

¹Institute for Climate and Atmospheric Science, School of Earth and Environment, University of Leeds, Leeds, UK

²National Centre for Atmospheric Science, School of Earth and Environment, University of Leeds, Leeds, UK

³National Oceanography Centre, Southampton, UK

⁴Cooperative Institute for Research in Environmental Sciences, University of Colorado and NOAA-Earth System Research Laboratory, Boulder, CO, USA

⁵Department of Meteorology and the Bolin Centre for Climate Research, Stockholm University, Stockholm, Sweden

Received: 3 August 2015 – Accepted: 24 August 2015 – Published: 10 September 2015

Correspondence to: P. Achtert (p.achtert@leeds.ac.uk)

Published by Copernicus Publications on behalf of the European Geosciences Union.

Title Page

Abstract

Introduction

Conclusions

References

Tables

Figures



Back

Close

Full Screen / Esc

Printer-friendly Version

Interactive Discussion



Abstract

Three months of Doppler lidar wind measurements were obtained during the Arctic Cloud Summer Experiment on the icebreaker *Oden* during the summer of 2014. Such ship-borne measurements require active stabilisation to remove the effects of ship motion. We demonstrate that the combination of a commercial Doppler lidar with a custom-made motion-stabilisation platform enables the retrieval of wind profiles in the Arctic boundary layer during both cruising and ice-breaking with statistical uncertainties comparable to land-based measurements. This holds particularly within the planetary boundary layer even though the overall aerosol load was very low. Motion stabilisation was successful for high wind speeds in open water and the resulting wave conditions. It allows for the retrieval of winds with a random error below 0.2 m s^{-1} , comparable to the measurement error of standard radiosondes. The combination of a motion-stabilised platform with a low-maintenance autonomous Doppler lidar has the potential to enable continuous long-term high-resolution ship-based wind profile measurements over the oceans.

1 Introduction

Profiles of wind speed and direction are one of the most fundamental quantities for meteorological studies. Radiosoundings are still the primary source of global wind profiles (WMO, 2012); however, unless exceptional measures are taken to enable simultaneous reception from multiple sondes, they can only provide a time resolution of the order of hours. This may be adequate to provide a reference measurement of general conditions, but for detailed studies of boundary layer processes continuous and much higher time resolution wind profiles are required. Furthermore, radiosounding stations for routine operational observations are mostly land-based. Observations at remote sites are very sparse and almost non-existent over the oceans. Any additional observations in data-sparse regions are valuable to improve the initial conditions for numerical weather

AMTD

8, 9339–9372, 2015

Ship-borne wind profiling with lidar

P. Achtert et al.

Title Page

Abstract

Introduction

Conclusions

References

Tables

Figures



Back

Close

Full Screen / Esc

Printer-friendly Version

Interactive Discussion



forecasts (Houchi et al., 2010; WMO, 2012; Baker et al., 2014) and for assimilation into reanalysis products for climate research (e.g. Dee et al., 2011).

Over the ocean, remote sensing with a ship-based Doppler lidar provides an attractive alternative to radiosoundings for obtaining profiles with a high time resolution (Baker et al., 2014). However, a number of technical challenges must be overcome to obtain high quality measurements. Ship motion, both its mean horizontal velocity when underway and the high frequency motions induced by waves and, in this study, ice-breaking, increases the random error of the raw measurements on a range of temporal scales. These errors may even be larger than the wind velocity being measured. In order to correct for the effects of ship motion, the constantly changing orientation and motion of the measurement platform must be compensated for. This can be done either by measuring the ship's motions and correcting for this after the fact, or by actively stabilising the instrument for these motions. If the time taken to make a single along-beam Doppler velocity measurement is long enough for the ship motion to change significantly then active motion stabilisation of the instrument is required. Only a few studies have used Doppler lidar on ships, and fewer still have actively stabilised the system against ship motions. Improvements in technology along with decreasing costs make this an increasingly attractive approach.

Wolfe et al. (2007) and Pichugina et al. (2012) report on a deployment of the NOAA High Resolution Doppler Lidar (HRDL) at sea during the New England Air Quality Study in 2004, along with the first use of a motion compensation system. The motion system combined GPS data with 6-axis accelerometers and rate gyros integrated over time to determine the orientation and motion of the lidar in real time. This information was then used to actively compensate the orientation of the lidar's scanning unit for the ship's motion. The platform velocity component along the lidar beam was calculated and subsequently removed from the Doppler velocity measurement. A pointing accuracy of order 1° was achieved under typical conditions during the cruise. Subsequent deployments (Tucker et al., 2009) improved on this, achieving an accuracy of $\approx 0.5^\circ$. The estimated noise introduced into each line-of-sight velocity measurement by the motion

Ship-borne wind profiling with lidar

P. Achtert et al.

Title Page

Abstract

Introduction

Conclusions

References

Tables

Figures



Back

Close

Full Screen / Esc

Printer-friendly Version

Interactive Discussion



correction was 0.3 ms^{-1} ; averaging over a 3 min interval reduced this to 0.015 ms^{-1} , with a mean bias of 0.05 ms^{-1} .

Here we present measurements with a motion-stabilised commercial scanning Doppler lidar. Lacking real-time control of the scanning head orientation, as used by Wolfe et al. (2007) and Pichugina et al. (2012), we mount the lidar as a whole in a motion-stabilised platform. The instrument was operated near-continuously over a period of 3 months on a ship in the Arctic Ocean during the summer and autumn of 2014. The wind measurements are compared to 6-hourly radiosoundings and measurements from a sonic anemometer mounted on a mast over the bow of the ship. We give a description of the design and operation of the motion stabilisation platform together with the lidar in Sect. 2. Section 3 presents the evaluation of the lidar wind measurements, an investigation of the measurement error of the motion-stabilised instrument, and the effect of flow distortions caused by the ship. The paper closes with a discussion and summary in Sect. 4.

2 Measurements

The measurements presented here are drawn from the Arctic Cloud Summer Experiment (ACSE), part of the *Swedish-Russian-US Arctic Ocean Investigation on Climate-Cryosphere-Carbon (SWERUS-C³)*, which undertook a 3 month long cruise on the icebreaker *Oden*. Sailing from Tromsø, Norway, on 5 July 2014, the cruise followed the Siberian Shelf to cross the Barents, Kara, Laptev, and East Siberian Seas to arrive in Barrow, Alaska, on 19 August 2014. The return leg departed Barrow on 20 August 2014 and followed a similar route, slightly further north, back to Tromsø, arriving on 5 October 2014 (Fig. 1). ACSE ran an extensive suite of in situ and remote sensing instrumentation throughout the full 3 months of the cruise (Tjernström et al., 2015). Here, we focus on measurements with a scanning Doppler lidar and 6-hourly radiosoundings.

Ship-borne wind profiling with lidar

P. Achtert et al.

Title Page

Abstract

Introduction

Conclusions

References

Tables

Figures



Back

Close

Full Screen / Esc

Printer-friendly Version

Interactive Discussion



2.1 Doppler lidar

The lidar used here is a HALO Photonics Stream Line scanning micro-pulsed Doppler lidar (<http://halo-photonics.com/>, Pearson et al., 2009) that was located on the roof of a container above the laboratory space on the foredeck of *Oden* (Fig. 2, left) at a height of 12 m a.s.l. The instrument operates at a wavelength of 1.55 μm and uses cloud droplets and aerosols as a tracer for air motion. Cloud layers with significant droplet concentrations produce full signal attenuation, prohibiting the acquisition of data above. Such liquid layers were frequently found near 400–500 m a.s.l. in this Arctic marine environment. The lidar's range resolution is 18 m, with 533 range gates and a maximum measurement distance of 9.6 km; the Doppler velocity resolution is 0.0382 ms^{-1} . An overview of the system parameters is presented in Table 1. Throughout the cruise the lidar was configured to undertake several different scan patterns on a fixed cycle. The wind profile scan ran every 10 min, using a 5-point measurement: a vertical beam and 4 off-vertical measurements at an elevation angle of 70° and azimuth angles at 90° increments. The measurement of velocity along each beam is comprised of 30 000 pulses at 15 kHz, and is thus an average over a 2 s interval. The time taken for the scanning head to move between consecutive beam positions is also approximately 2 s. All the individual measurements used in the calculation of a single wind profile thus take place within a period of approximately 20 s.

2.2 Ship motion stabilisation

The lidar was stabilised against the pitch and roll of the ship by mounting it within a specially constructed motion-stabilised frame (Fig. 2, right). To minimise the torque required, the whole system is balanced so that the axes of rotation pass through the centre of mass of the instrument. The motion of the ship and of the lidar are measured with two Xsens MTi-700-G attitude and heading reference system (AHRS) sensors rigidly mounted to the outer- and inner-most frames, respectively. The motion-control algorithm takes the raw measurements of the rates of rotation for pitch and roll from the

Ship-borne wind profiling with lidar

P. Achtert et al.

Title Page

Abstract

Introduction

Conclusions

References

Tables

Figures



Back

Close

Full Screen / Esc

Printer-friendly Version

Interactive Discussion



Ship-borne wind profiling with lidar

P. Achtert et al.

Title Page

Abstract

Introduction

Conclusions

References

Tables

Figures



Back

Close

Full Screen / Esc

Printer-friendly Version

Interactive Discussion



ship-frame sensor. It drives servo motors at the same rate but in the opposite direction to hold the inner frame steady against the pitch and roll of the ship. This will maintain the orientation with respect to the horizontal that it had when the system started up. In order to force the inner frame towards the horizontal, the specified rates of rotation are modified by the addition of factors proportional to the absolute pitch and roll of the inner-frame. The measurement of the inner-frame attitude uses the solution calculated internally by the Xsens AHRS via a proprietary algorithm which combines all its raw measurements using a Kalman filter. The complete measurement and control cycle runs at 10 Hz. Both the lidar data logging system and the motion control system are synchronised to UTC via the ship's time server.

Approximately half of the ACSE cruise took place in sea ice where the ship's pitch and roll are modest (typically less than 2°) but ship motions can be sudden when breaking ice; the other half was in open water, sometimes near the ice edge and other times hundreds of kilometres distant. Some extensive periods during the second leg were spent in open water under conditions of moderately high winds (10 m winds up to 17 m s^{-1}) and waves up to several metres. The *Oden* is designed primarily for working within sea ice and lacks a keel; it thus has rather poor stability in rough seas and suffers significant roll motions. Figure 3a shows a short portion of the time series of roll angles for the ship and the motion-stabilised lidar from 18 September, during the period of roughest seas encountered, when the greatest ship motion was experienced. The probability distribution of lidar roll angle for the 1 h period with greatest ship roll is shown in Fig. 3b. The maximum ship roll approaches $\pm 8^\circ$ with a period of approximately 8.5 s. The motion stabilised frame keeps the lidar within 0.3° of horizontal 96.5 % of the time, and within 0.5° of horizontal 99.3 % of the time. At no point does the lidar roll angle exceed 0.9° .

The residual attitude and 3-dimensional velocity of the stabilised inner frame were calculated and combined with the lidar beam orientation to correct the line-of-sight Doppler velocity measurement for the ship's velocity along the beam. In principle the complete platform attitude and velocity solution could be obtained directly from the

Ship-borne wind profiling with lidar

P. Achtert et al.

Title Page

Abstract

Introduction

Conclusions

References

Tables

Figures



Back

Close

Full Screen / Esc

Printer-friendly Version

Interactive Discussion



the commonly used threshold of -20 dB. This amounts to rejecting a total of 75 % of all individual data points that do not fulfill the SNR criterion. Note that data rejection varies greatly with altitude and atmospheric conditions, and is highest in the free troposphere where the majority of rejected data points lie. This rejection rate is particularly high for our Arctic observations as we cannot rely on the abundance of scatterers that lead to generally better SNR in observations at mid-latitudes. It is likely that changing the telescope focal length from infinity to 1–2 km (Hirsikko et al., 2014) would improve data collection for conditions of low aerosol load as encountered during ACSE. Unfortunately, the older model of HALO lidar used in ACSE did not allow for overlap adjustment as easily as its successor, and this adjustment was therefore not made.

Wind speed and direction were obtained from the motion corrected HALO Doppler lidar measurements using both the five-point geometrical wind solution and the 4-point sinusoidal fit method described in Werner (2005), assuming no major changes or air motion occur within the scanning volume (Lane et al., 2013). For the 4-point sinusoidal fit method, we applied the quality assurance criteria described in Päsckhe et al. (2015). This methodology tests for horizontal homogeneity of the wind field (we applied a threshold of $R^2 > 0.95$) and the collinearity of the Doppler velocity measurements used within one scan. For the latter, we ensured that measurements with gaps in the azimuth scan of larger than 210° were not included for further data analysis, i.e. scans with less than three out of four points available for analysis.

We also investigated the influence of changes in the heading of the ship during individual scan cycles with and without applying the quality assurance criteria of Päsckhe et al. (2015). These criteria remove any dependence of wind speed on the change in the ship's heading between the first and the last measurement used in the retrieval. The issue will be addressed in more detail in Sect. 3.1.

Continuous wind profiles could be retrieved up to a maximum altitude of 1600 m a.s.l. during cloud-free conditions. Data coverage is highest in the lowermost 200 m (93 %) and decreases exponentially with height to 13 % at 1000 m. This is less than usually observed with the same type of instrument at mid-latitudes (Pearson et al., 2009;

**Ship-borne wind
profiling with lidar**

P. Achtert et al.

Title Page

Abstract

Introduction

Conclusions

References

Tables

Figures



Back

Close

Full Screen / Esc

Printer-friendly Version

Interactive Discussion



Päschke et al., 2015) due to the generally very low aerosol load in the Arctic (e.g. Lan-
nefors et al., 1983; Heintzenberg and Leck, 2012; Birch et al., 2012). However, within
the boundary layer we yield data coverage comparable to previous studies. Averaged
over all observations, we find that the maximum height of useful wind data is around
100 m lower for cloudy (but not fully attenuating) conditions than for cloud-free condi-
tions. Most of the observed clouds showed a base height of 300 m or less. Fog was
frequently observed during the first leg of the cruise, with fewer fog cases encountered
during the second leg. Such conditions typically lead to full attenuation of the lidar sig-
nal within the fog. The presence of multiple semi-transparent cloud layers allows for
measurements of up to 3000 m on some occasions, leading to data coverage of 5 % at
this altitude.

In order to assess the accuracy of the lidar wind retrievals, results have been com-
pared to the 6-hourly radiosoundings. We used Vaisala RS92 radiosondes with a nom-
inal ascent rate of 4 ms^{-1} . The manufacturer gives a measurement uncertainty of
 0.15 ms^{-1} and 2° for wind speed and direction, respectively (VAISALA, 2015). Wind
profiles from lidar and radiosoundings were interpolated to a common height grid. In
addition, lidar winds were averaged over at least 2 scans in the first 30 min after the
launch of the radiosonde.

To increase the amount of data for comparison, wind speed has also been compared
to sonic anemometer measurements that were extrapolated to 75 m height following
the method of Smith (1988) using the neutral drag coefficient, wind speed and surface
and air temperatures. A Metek USA-1 sonic anemometer was mounted approximately
20.6 m above the water line on a lattice mast installed over the bow (Fig. 2, left). It
features a heated sensing head that enables measurements even in severe icing con-
ditions. The motion of the anemometer was monitored with an Xsens MTi-G-700 AHRS
mounted at its base. The measurements were corrected for attitude and ship motion
following Edson et al. (1998) as well as for the mean wind speed bias and flow height
adjustment induced by flow distortion over the ship (Yelland et al., 2002; Moat et al.,

2005). The latter correction uses results from a computational fluid dynamics (CFD) modelling study of the *Oden* undertaken specifically for this campaign.

The height of 75 m for comparison to the lidar observations was chosen as few lidar measurements below 75 m height passed the quality-assurance criteria. Strictly speaking the logarithmic wind profile should extend only through the surface layer – approximately the lowest 10 % of the boundary layer. We would expect, however, that the wind speed in the lower half of the boundary layer would be very close to that at the top of the surface layer. Here we restrict this comparison to cases for which the boundary layer depth exceeds 200 m so that the 75 m level is well within the lower half of the boundary layer; we estimate that any bias resulting from the extrapolation to this level is less than 10 % of the wind speed at the height of the anemometer. The boundary layer depth was determined from Ceilometer measurements (Vaisala CL31) on *Oden* using the STRAT-2D algorithm (Morille et al., 2007; Haeffelin et al., 2012). Measurements from the lidar were interpolated to the 20 min averaging interval of the sonic anemometer for the comparison.

3 Results

3.1 Lidar winds evaluation

Figure 4 shows scatter plots of wind-speed and direction for lidar vs. radiosonde using the 4-point sinusoidal fit solution at an altitude of 75 m a.s.l.; and lidar vs. sonic anemometer for wind speed only. The lidar and radiosonde wind directions agree very well for both methods ($R^2 = 0.96$ for 5-point geometrical wind solution (not shown) and $R^2 = 0.99$ for 4-point sinusoidal fit; see Table 2) and shows negligible bias (Fig. 4a). Extreme outliers (red points in Fig. 4a and b) were determined through the Grubbs test (Grubbs, 1969) and excluded from the linear fits. The values at around 0 and 360° in Fig. 4a are related to the periodicity of wind direction and do not represent erroneous measurements per se. The sinusoidal fit of 75 m lidar winds to the radiosonde winds

Ship-borne wind profiling with lidar

P. Achtert et al.

Title Page

Abstract

Introduction

Conclusions

References

Tables

Figures



Back

Close

Full Screen / Esc

Printer-friendly Version

Interactive Discussion



Ship-borne wind profiling with lidar

P. Achtert et al.

Title Page

Abstract

Introduction

Conclusions

References

Tables

Figures



Back

Close

Full Screen / Esc

Printer-friendly Version

Interactive Discussion



(Fig. 4b) gives a larger intercept than that to the extrapolated anemometer wind speeds (Fig. 4c), with the lidar slightly underestimating the radiosondes for winds below about 4 ms^{-1} and overestimating at higher wind speed – by about 2 ms^{-1} at wind speeds of 16 ms^{-1} . The lidar slightly overestimates compared with the extrapolated anemometer wind speeds, but by less than 0.5 ms^{-1} at the highest winds. $R^2 = 0.86$ for fits to both radiosonde and sonic anemometer winds. These results compare well with those of (Wolfe et al., 2007; Pichugina et al., 2012), who compared profiles of zonal and meridional wind derived from full 360° velocity-azimuth display (VAD) scans of the HRDL lidar with radiosonde profiles.

Linear fit parameters for the comparison of wind speed from lidar and extrapolated sonic measurements for different boundary layer depths are given in Table 3. Linear fit parameters for both geometric and sinusoidal fits, as well as the number of measurements for the comparisons shown in Fig. 4, are given in Table 2.

Both the 5-point geometrical and sinusoidal methods to derive wind speed and direction from the lidar data yield similar results. However, the sinusoidal fit is of advantage for our application as it only requires three input points to provide a solution. This increases the number of measurement intervals that can be used by around 25%. Consequently, sinusoidal fits have been used in the analysis of Doppler lidar measurements during the ACSE cruise. The blue diamonds in Fig. 4a and b represent observations during which the motion-stabilization platform was not operating. While these are only five individual scans, they do demonstrate that an unstabilised instrument suffers far greater scatter in the measurements.

Figure 5 (blue lines) shows a height-resolved view of the correlation coefficient for the different comparisons between lidar winds and the soundings. The squared correlation coefficient for wind direction is approximately 0.99 and almost constant with altitude up to 40 m a.s.l., decreasing slightly to approximately 0.97 at 700 m a.s.l. For wind speed the squared correlation coefficient's minimum (0.86 to 0.89) is a minimum at the lowest altitudes and it improves with height to values comparable to that for wind direction.

Too few data points are available at altitudes higher than 700 m.a.s.l. for an effective comparison.

The squared correlation coefficient for the solution for wind speed improves from 0.86 at 100 to 0.94 at 400 m. In addition, the bias decreases from 0.48 to 0.14 ms⁻¹.

A detailed overview of the correlation parameters is given in Table 4. A similar improvement (with respect to values obtained using the quality assurance criterion of Päsche et al., 2015) in the comparison to the radiosonde is obtained when the change in the ship's heading during one scan is restricted to smaller angles of 5 or 10° rather than 20°. This is expressed by the red and black lines for different cut-off angles presented in Fig. 5. Large changes of the heading of the ship shifts the azimuth angles used in the 4-point sinusoidal fit and leads to non-uniform intervals; this can lead to a degradation of the fit.

There are a number of effects that might influence the measurements at low level. The primary source of discrepancy is likely to be the fundamentally different nature of the measurements. The radiosonde follows a unique trajectory resulting from the sum of its buoyant ascent rate and the motion of the air it ascends through. Within the boundary layer, turbulence superimposes chaotic perturbations about the mean flow; the largest scale eddies might result in very different trajectories depending on the precise time and location of launch. The lidar, on the other hand, calculates a wind profile from the air motions along each beam, which are separated both in time and in space – increasingly so with increasing altitude, while the sonic anemometer measures the velocity within a small localised sampling volume, with all components being sampled with a period (0.05 s) short enough to be considered instantaneous compared to the lidar. These effects, along with the increasing spatial separation between the radiosonde and the lidar may also cause the slight decrease in the correlation for wind direction with increasing altitude. An additional source of discrepancies is flow distortion around the ship; this would influence low-level measurements from all three systems, with different effects on each due to their different locations.

Ship-borne wind profiling with lidar

P. Achtert et al.

Title Page

Abstract

Introduction

Conclusions

References

Tables

Figures



Back

Close

Full Screen / Esc

Printer-friendly Version

Interactive Discussion



Ship-borne wind profiling with lidar

P. Achtert et al.

Title Page

Abstract

Introduction

Conclusions

References

Tables

Figures



Back

Close

Full Screen / Esc

Printer-friendly Version

Interactive Discussion



The radiosonde will furthermore take time to accelerate to the ambient wind speed following launch, and can suffer from pendulum motions as the tether unwinds after launch. The latter effect can be particularly pronounced during high wind speed conditions and might affect the calculation of wind speed from consecutive GPS position estimates. The sondes are also launched close to the ship's superstructure and depending on the ship-relative wind direction, may have been launched from within the local wind-shadow of the ship's superstructure, delaying its acceleration to match the wind; for a short while after launch its motion can also be affected by the turbulent wake of the ship. The radiosondes' low-level winds are also affected by the surface winds entered into the proprietary sounding program; these were obtained from the sonic anemometer measurements, and again, depending on ship-relative wind direction, may suffer some distortion from the true value.

Time series of wind speed and direction at an altitude of 100 m as measured with radiosonde and lidar are shown in Fig. 6. The gap from 4 to 12 August 2014 is due to a change in scanning setup of the lidar; no retrieval of wind speed and direction is possible during this period. During the first leg, the mean horizontal wind speed was 7.2 m s^{-1} , while a slightly larger value of 9.0 m s^{-1} was obtained for the second leg. Wind direction showed high variability throughout the cruise. However, extensive periods of northerly and south-easterly winds can be identified. The relative difference presented in the bottom panel of Fig. 6 shows that wind direction generally agrees within 10%. A stronger spread of values is found for the relative difference of wind speed with extreme values of up to 50% difference. For the average wind speed of 6 to 8 m s^{-1} and above, the difference between lidar and radiosonde is below 20%. The mean (median) winds speeds at 100 m a.s.l. are 7.9 ± 3.4 (7.7) m s^{-1} and 8.2 ± 3.5 (8.1) m s^{-1} for the lidar and radiosonde, respectively. The relative difference in wind speed follows a Gaussian distribution (not shown) that is centred slightly off zero as winds measured by lidar are on average 0.3 m s^{-1} lower than those inferred from the radiosoundings.

3.2 Measurement uncertainty

Following the approach of Frehlich (2001) and Pearson et al. (2009), an auto-covariance scheme has been used to determine the standard deviation of the measurements with the motion-stabilised lidar during ACSE. The difference between the zeroth lag (first term in the auto-covariance) and the first lag gives a measure of the random error. This value has to be compared to the theoretical standard deviation of the instrument. The theoretical standard deviation has been estimated for SNR values between -30 and 16 dB as described in O'Connor et al. (2010). We used lidar specifications given in Table 1 and a signal spectral width of 2 ms^{-1} (O'Connor et al., 2010). To determine the standard deviation for observations during ACSE, we only considered wind profiles during relatively steady wind conditions, i.e. during periods for which at least four consecutive lidar wind profiles showed a mean vertical velocity within $\pm 0.25 \text{ ms}^{-1}$ of zero.

The observed standard deviation of the vertical velocity as a function of SNR is presented in Fig. 7 together with the theoretical standard deviation calculated as described above. We find a constant random error range between 0.025 and 0.2 ms^{-1} above -16 dB. This confirms our choice of a conservative SNR threshold of -16 dB according to the method of Päsche et al. (2015). SNR larger than 2 dB refer to cloud measurements. The error increases for lower SNR as the result of increasing signal noise. The experimental error exceeds the theoretical values but follows the expected change with SNR. Pearson et al. (2009) reported an error between 0.03 and 0.04 ms^{-1} for SNR larger than -10 dB and errors that increase up to 0.4 ms^{-1} at -20 dB. Our findings compare well with Fig. 2c in Pearson et al. (2009). The larger standard deviation we observe in our measurements is likely to be the result of the low aerosol load in the Arctic in combination with the limitations of the motion stabilisation. The latter include the residual small perturbations about the horizontal and the necessity of correcting the Doppler velocity measurements for ship motion only as an average over the 2 s

Ship-borne wind profiling with lidar

P. Achtert et al.

Title Page

Abstract

Introduction

Conclusions

References

Tables

Figures



Back

Close

Full Screen / Esc

Printer-friendly Version

Interactive Discussion



measurement interval; during this time the high frequency ship motions, induced by waves or icebreaking, can change significantly.

To determine the bias of the measurements, we averaged all data for which steady wind conditions prevailed (about 3000 points at 200 m.a.s.l. decreasing down to 200 points at 1000 m.a.s.l.). While the average vertical velocity should be close to zero, we derived a mean value of $0.1365 \pm 0.005 \text{ ms}^{-1}$ for the height range up to 1000 m.a.s.l. This means that measurements of vertical velocity will be slightly biased upwards.

There are a number of potential sources of real bias in the measured vertical wind. One is the aliasing of horizontal wind into the vertical wind speed measurement as the result of imperfect motion stabilisation or misalignment of the lidar and AHRS units; the latter is estimated to be less than 0.5° . If the lidar alignment deviates from the horizontal by 0.3 or 0.9° (respectively the typical and maximum limits of the motion stabilisation) for a campaign mean wind speed of 8 ms^{-1} , the aliasing effect in the vertical wind will be ± 0.04 or $\pm 0.12 \text{ ms}^{-1}$, respectively. A source of a real upward air motion over the lidar is flow distortion over the ship. This is known to be a cause of significant bias in estimates of the mean wind (Yelland et al., 1998; Moat et al., 2006b, a; Moat and Yelland, 2008) and is now often corrected using the results of CFD modelling studies of the flow over ships (Yelland et al., 2002; Moat et al., 2005, 2006b, a; Moat and Yelland, 2008).

3.3 Effect of flow distortion

A CFD study of flow over the *Oden* was undertaken in order to determine corrections to the mean wind measured on the foremast and hence for the estimates of turbulent exchange coefficients. Here we utilise these model fields, along with some additional model runs, to examine the biases resulting from flow distortion over the lidar location. A commercial CFD code, VECTIS (Ricardo, 2014), was used to model the 3-dimensional flow over the *Oden* for a wide range of wind directions: every 10° from bow-on flow, through beam-on flow on both port and starboard sides. Additional runs were undertaken for flow from 120 , 150 and 180° from the bow. All runs used

Ship-borne wind profiling with lidar

P. Achtert et al.

Title Page

Abstract

Introduction

Conclusions

References

Tables

Figures



Back

Close

Full Screen / Esc

Printer-friendly Version

Interactive Discussion



Ship-borne wind profiling with lidar

P. Achtert et al.

Title Page

Abstract

Introduction

Conclusions

References

Tables

Figures



Back

Close

Full Screen / Esc

Printer-friendly Version

Interactive Discussion



a 10 m wind speed of 7 ms^{-1} , close to the campaign mean, with one additional (bow on) run being undertaken for $U_{10} = 15 \text{ ms}^{-1}$. The stratification is neutral, free stream wind profiles are logarithmic with altitude and the far field vertical velocity is zero. The model domain is centred on the ship and extends 1000 m in length, 1800 m in width, and 250 m in height. The number of computational cells within the domain was around 5 million. The cell size varied throughout the domain, with sizes of 0.12 to 0.25 m at the bow mast instrument location. This increased to around 20 m close to the edges of the domain. A grid independency study showed that a 50 % reduction of cell sizes over the whole domain only resulted in a 1 % change in wind speed bias with respect to the free stream flow at the bow mast anemometer locations.

The ship imposes a significant obstacle to the flow, and forces a strong vertical velocity in the lowest few 10 s of metres above the lidar, which varies with wind direction (Fig. 8a). This effect is slightly asymmetric about the bow because the lidar is situated towards the port side. At 75 m, the lowest level of robust Doppler wind measurements, the vertical velocity varies from about 0.2 to 0.4 ms^{-1} for $U_{10} = 7 \text{ ms}^{-1}$ and for wind directions for which the superstructure does not directly block the flow; this decreases approximately exponentially with altitude. The mean calculated vertical velocity above 75 m (roughly three times the obstacle height) is 0.04 ms^{-1} for flow onto the bow, increasing to a little over 0.12 ms^{-1} for beam-on flow. The CFD run with $U_{10} = 15 \text{ ms}^{-1}$ for bow-on flow showed vertical velocity approximately double that at $U_{10} = 7 \text{ ms}^{-1}$. The altitude-dependent vertical wind speed behaviour derived from CFD modelling was also observed in the Doppler lidar measurements, though with smaller magnitude as a result of temporal averaging of turbulent motions and vertical smoothing.

The vertical velocity at the top of the model domain at 250 m is set to zero; in reality a small vertical velocity might extend above this level. The normalised difference between the horizontal wind speed and the far field wind at the top of the domain is non-zero but less than 0.5 % (Fig. 8b), whereas we would expect it to approach zero. This is due to the ship slightly constricting the flow within the domain. Overall the nor-

malised bias in horizontal wind speed is less than 2 % for all wind directions at altitudes above 75 m.

4 Conclusions and summary

We have presented Doppler lidar measurements made during the Arctic cruise of the icebreaker *Oden* in summer and autumn 2014. In contrast to earlier shipborne observations in which data on ship motion was used to correct the alignment of the scanning unit of a Doppler lidar, we placed the instruments on a motion-stabilisation platform that enabled active stabilisation to within 0.3° of horizontal most of the time. Our setup allows for the retrieval of winds that are in good agreement with both radiosoundings and extrapolated measurements from an anemometer on the foremast. The comparison of the stabilised HALO Doppler lidar to independent measurements is comparable to that in land-based investigations (Barlow et al., 2011; Hirsikko et al., 2014; Päsche et al., 2015).

The fundamental measurement error of the lidar wind speed was found to be in the range from 0.025 to 0.2 ms^{-1} for SNR above -16 dB , which is smaller than the discrepancy between the mean wind speed derived from lidar and radiosoundings of 0.3 ms^{-1} (see Sect. 3.1). Overall, lidar measurements increase in reliability when change in ship's heading within a 20 s measurement cycle is at a minimum. The measurement range during fog-free periods was limited primarily by low aerosol concentration limiting the backscatter in clear air; measurements were obtained up to an altitude of 1000 m a.s.l., and up to 3000 m a.s.l. when multiple layers of transparent clouds were present. Higher altitudes would be reached at mid-latitudes where atmospheric aerosol load is generally higher than in the Arctic (Wolfe et al., 2007; Pearson et al., 2009; Päsche et al., 2015). Data coverage was found to be comparable to previous land- and ship-based Doppler lidar observations. Ship-based Doppler lidar measurements provide a much more detailed, higher time-resolution view of boundary-layer processes than can be achieved with radiosondes. At sea and on other moving platforms, mo-

Ship-borne wind profiling with lidar

P. Achtert et al.

Title Page

Abstract

Introduction

Conclusions

References

Tables

Figures



Back

Close

Full Screen / Esc

Printer-friendly Version

Interactive Discussion



**Ship-borne wind
profiling with lidar**

P. Achtert et al.

Title Page

Abstract

Introduction

Conclusions

References

Tables

Figures



Back

Close

Full Screen / Esc

Printer-friendly Version

Interactive Discussion



cloud and their response to CCN in the central Arctic: ASCOS case studies, *Atmos. Chem. Phys.*, 12, 3419–3435, doi:10.5194/acp-12-3419-2012, 2012. 9347

Brooks, I. M.: Spatially distributed measurements of platform motion for the correction of ship-based turbulent fluxes, *J. Atmos. Ocean. Tech.*, 25, 2007–2017, doi:10.1175/2008JTECHA1086.1, 2008. 9345

Dee, D. P., Uppala, S. M., Simmons, A. J., Berrisford, P., Poli, P., Kobayashi, S., Andrae, U., Balmaseda, M. A., Balsamo, G., Bauer, P., Bechtold, P., Beljaars, A. C. M., van de Berg, L., Bidlot, J., Bormann, N., Delsol, C., Dragani, R., Fuentes, M., Geer, A. J., Haimberger, L., Healy, S. B., Hersbach, H., Hólm, E. V., Isaksen, I., Kållberg, P., Köhler, M., Matricardi, M., McNally, A. P., Monge-Sanz, B. M., Morcrette, J.-J., Park, B.-K., Peubey, C., de Rosnay, P., Tavolato, C., Thépaut, J.-N., and Vitart, F.: The ERA-Interim reanalysis: configuration and performance of the data assimilation system, *Q. J. Roy. Meteor. Soc.*, 137, 553–597, doi:10.1002/qj.828, 2011. 9341

Drennan, W., Graber, H., Collins III, C., Herrera, A., Potter, H., Ramos, R., and Williams, N.: EASI: an air-sea interaction buoy for high winds, *J. Atmos. Ocean. Tech.*, 31, 1397–1409, doi:10.1175/JTECH-D-13-00201.1, 2014. 9345

Edson, J. B., Hinton, A. A., Prada, K. E., Hare, J. E., and Fairall, C. W.: Direct covariance flux estimates from mobile platforms at sea*, *J. Atmos. Ocean. Tech.*, 15, 547–562, doi:10.1175/1520-0426(1998)015<0547:DCFEFM>2.0.CO;2, 1998. 9345, 9347

Frehlich, R.: Estimation of velocity error for Doppler lidar measurements, *J. Atmos. Ocean. Tech.*, 18, 1628–1639, doi:10.1175/1520-0426(2001)018<1628:EOVEFD>2.0.CO;2, 2001. 9352

Grubbs, F. E.: Procedures for detecting outlying observations in samples, *Technometrics*, 11, 1–21, doi:10.1080/00401706.1969.10490657, 1969. 9348

Haefelin, M., Angelini, F., Morille, Y., Martucci, G., Frey, S., Gobbi, G., Lolli, S., O'Dowd, C., Sauvage, L., Xueref-Rémy, I., Wastine, B., and Feist, D.: Evaluation of mixing-height retrievals from automatic profiling lidars and ceilometers in view of future integrated networks in Europe, *Bound.-Lay. Meteorol.*, 143, 49–75, doi:10.1007/s10546-011-9643-z, doi:10.1007/s10546-011-9643-z, 2012. 9348

Heintzenberg, J. and Leck, C.: The summer aerosol in the central Arctic 1991–2008: did it change or not?, *Atmos. Chem. Phys.*, 12, 3969–3983, doi:10.5194/acp-12-3969-2012, 2012. 9347

**Ship-borne wind
profiling with lidar**

P. Achtert et al.

Title Page

Abstract

Introduction

Conclusions

References

Tables

Figures



Back

Close

Full Screen / Esc

Printer-friendly Version

Interactive Discussion



- Hirsikko, A., O'Connor, E. J., Komppula, M., Korhonen, K., Pfüller, A., Giannakaki, E., Wood, C. R., Bauer-Pfundstein, M., Poikonen, A., Karppinen, T., Lonka, H., Kurri, M., Heinonen, J., Moisseev, D., Asmi, E., Aaltonen, V., Nordbo, A., Rodriguez, E., Lihavainen, H., Laaksonen, A., Lehtinen, K. E. J., Laurila, T., Petäjä, T., Kulmala, M., and Viisanen, Y.: Observing wind, aerosol particles, cloud and precipitation: Finland's new ground-based remote-sensing network, *Atmos. Meas. Tech.*, 7, 1351–1375, doi:10.5194/amt-7-1351-2014, 2014. 9345, 9346
- Houchi, K., Stoffelen, A., Marseille, G., and De Kloe, J.: Comparison of wind and wind shear climatologies derived from high-resolution radiosondes and the ECMWF model, *J. Geophys. Res.-Atmos.*, 115, D22123, doi:10.1029/2009JD013196, 2010. 9341
- Landwehr, S., O'Sullivan, N., and Ward, B.: Direct flux measurements from mobile platforms at sea: motion and air-flow distortion corrections revisited, *J. Atmos. Ocean. Tech.*, 32, 1163–1178, doi:10.1175/JTECH-D-14-00137.1, 2015. 9345
- Lane, S., Barlow, J. F., and Wood, C. R.: An assessment of a three-beam Doppler lidar wind profiling method for use in urban areas, *J. Wind Eng. Ind. Aerod.*, 119, 53–59, doi:10.1016/j.jweia.2013.05.010, 2013. 9345, 9346
- Lannefors, H., Heintzenberg, J., and Hansson, H. C.: A comprehensive study of physical and chemical parameters of the Arctic summer aerosol; results from the Swedish expedition Ymer-80, *Tellus B*, 35, 40–54, doi:10.1111/j.1600-0889.1983.tb00006.x, 1983. 9347
- McGillis, W. R., Edson, J. B., Hare, J. E., and Fairall, C. W.: Direct covariance air-sea CO₂ fluxes, *J. Geophys. Res.-Oceans*, 106, 16729–16745, doi:10.1029/2000JC000506, 2001. 9345
- Moat, B. I. and Yelland, M. J.: Going with the flow: state of the art marine meteorological measurements on the new NERC research vessel, *Weather*, 63, 158–159, doi:10.1002/wea.184, 2008. 9353
- Moat, B. I., Yelland, M. J., Pascal, R. W., and Molland, A. F.: An overview of the airflow distortion at anemometer sites on ships, *Int. J. Climatol.*, 25, 997–1006, doi:10.1002/joc.1177, 2005. 9347, 9353
- Moat, B. I., Yelland, M. J., and Molland, A. F.: Quantifying the airflow distortion over merchant ships. Part II: Application of the model results, *J. Atmos. Ocean. Tech.*, 23, 351–360, doi:10.1175/JTECH1859.1, 2006a. 9353
- Moat, B. I., Yelland, M. J., Pascal, R. W., and Molland, A. F.: Quantifying the airflow distortion over merchant ships. Part I: Validation of a CFD model, *J. Atmos. Ocean. Tech.*, 23, 341–350, doi:10.1175/JTECH1858.1, 2006b. 9353

Ship-borne wind
profiling with lidar

P. Achtert et al.

Title Page

Abstract

Introduction

Conclusions

References

Tables

Figures



Back

Close

Full Screen / Esc

Printer-friendly Version

Interactive Discussion



Morille, Y., Haeffelin, M., Drobinski, P., and Pelon, J.: STRAT: an automated algorithm to retrieve the vertical structure of the atmosphere from single-channel lidar data, *J. Atmos. Ocean. Tech.*, 24, 761–775, doi:10.1175/JTECH2008.1, 2007. 9348

Norris, S. J., Brooks, I. M., Hill, M. K., Brooks, B. J., Smith, M. H., and Sproson, D. A. J.: Eddy covariance measurements of the sea spray aerosol flux over the open ocean, *J. Geophys. Res.-Atmos.*, 117, d07210, doi:10.1029/2011JD016549, 2012. 9345

O'Connor, E. J., Illingworth, A. J., Brooks, I. M., Westbrook, C. D., Hogan, R. J., Davies, F., and Brooks, B. J.: A method for estimating the turbulent kinetic energy dissipation rate from a vertically pointing Doppler lidar, and independent evaluation from balloon-borne in situ measurements, *J. Atmos. Ocean. Tech.*, 27, 1652–1664, doi:10.1175/2010JTECHA1455.1, 2010. 9352

Päschke, E., Leinweber, R., and Lehmann, V.: An assessment of the performance of a 1.5 μm Doppler lidar for operational vertical wind profiling based on a 1-year trial, *Atmos. Meas. Tech.*, 8, 2251–2266, doi:10.5194/amt-8-2251-2015, 2015. 9345, 9346, 9347, 9350, 9352, 9355, 9369

Pearson, G., Davies, F., and Collier, C.: An analysis of the performance of the UFAM pulsed Doppler lidar for observing the boundary layer, *J. Atmos. Ocean. Tech.*, 26, 240–250, doi:10.1175/2008JTECHA1128.1, 2009. 9343, 9345, 9346, 9352, 9355

Pichugina, Y. L., Banta, R. M., Brewer, W. A., Sandberg, S. P., and Hardesty, R. M.: Doppler lidar-based wind-profile measurement system for offshore wind-energy and other marine boundary layer applications, *J. Appl. Meteorol. Climatol.*, 51, 327–349, doi:10.1175/JAMC-D-11-040.1, 2012. 9341, 9349

Ricardo: VECTIS Computational Fluid Dynamics (Release 2014.2) users guide, Tech. rep., Ricardo Software Ltd., UK, available at: [http://www.software.ricardo.com/support/manuals/](http://www.software.ricardo.com/support/manuals/vectis/pdfs/2014.2/VECTIS_2014.2_Manual.pdf)
[vectis/pdfs/2014.2/VECTIS_2014.2_Manual.pdf](http://www.software.ricardo.com/support/manuals/vectis/pdfs/2014.2/VECTIS_2014.2_Manual.pdf) (last access: 3 August 2015), 2014. 9353

Schween, J. H., Hirsikko, A., Löhnert, U., and Crewell, S.: Mixing-layer height retrieval with ceilometer and Doppler lidar: from case studies to long-term assessment, *Atmos. Meas. Tech.*, 7, 3685–3704, doi:10.5194/amt-7-3685-2014, 2014. 9345

Smith, S. D.: Coefficients for sea surface wind stress, heat flux, and wind profiles as a function of wind speed and temperature, *J. Geophys. Res.-Oceans*, 93, 15467–15472, doi:10.1029/JC093iC12p15467, 1988. 9347, 9363

Tjernström, M., Shupe, M. D., Brooks, I. M., Persson, P. O. G., Prytherch, J., Salisbury, D. J., Sedlar, J., Achtert, P., Brooks, B. J., Johnston, P. E., Sotiropoulou, G., and Wolfe, D.: Warm-

Ship-borne wind profiling with lidar

P. Achtert et al.

Title Page

Abstract

Introduction

Conclusions

References

Tables

Figures



Back

Close

Full Screen / Esc

Printer-friendly Version

Interactive Discussion



air advection, air mass transformation and fog causes rapid ice melt, *Geophys. Res. Lett.*, 42, 5594–5602, doi:10.1002/2015GL064373, 2015GL064373, 2015. 9342

Tucker, S. C., Senff, C. J., Weickmann, A. M., Brewer, W. A., Banta, R. M., Sandberg, S. P., Law, D. C., and Hardesty, R. M.: Doppler lidar estimation of mixing height using turbulence, shear, and aerosol profiles, *J. Atmos. Ocean. Tech.*, 26, 673–688, doi:10.1175/2008JTECHA1157.1, 2009. 9341

VAISALA: Radiosonde RS92-SGP, data sheet, available at: <http://www.vaisala.com/Vaisala%20Documents/Brochures%20and%20Datasheets/RS92SGP-Datasheet-B210358EN-F-LOW.pdf>, last access: 19 April 2015. 9347

Werner, C.: Doppler Wind Lidar, edited by: Weitkamp, Springer, New York, 325–353, 2005. 9346

WMO: Statement of guidance for global numeric weather prediction (NWP), available at: www.wmo.int/pages/prog/www/OSY/GOS-RRR.html (last access: 30 June 2015), 2012. 9340, 9341

Wolfe, D. E., Brewer, W. A., Tucker, S. C., White, A. B., White, D. E., Welsh, D. C., Ruffieux, D., Fairall, C. W., Ratterree, M., Intrieri, J. M., McCarty, B. J., and Law, D. C.: Shipboard multisensor merged wind profiles from the New England Air Quality Study 2004, *J. Geophys. Res.-Atmos.*, 112, d10S15, doi:10.1029/2006JD007344, 2007. 9341, 9349, 9355

Yang, M., Blomquist, B. W., and Nightingale, P. D.: Air-sea exchange of methanol and acetone during HiWinGS: Estimation of air phase, water phase gas transfer velocities, *J. Geophys. Res.-Oceans*, 119, 7308–7323, doi:10.1002/2014JC010227, 2014. 9345

Yelland, M., Moat, B. I., Taylor, P. K., Pascal, R. W., Hutchings, J., and Cornell, V. C.: Wind stress measurements from the open ocean corrected for airflow distortion by the ship, *J. Phys. Oceanogr.*, 28, 1511–1526, doi:10.1175/1520-0485(1998)028<1511:WSMFTO>2.0.CO;2, 1998. 9353

Yelland, M., Moat, B., Pascal, R., and Berry, D.: CFD model estimates of the airflow distortion over research ships and the impact on momentum flux measurements, *J. Atmos. Ocean. Tech.*, 19, 1477–1499, doi:10.1175/1520-0426(2002)019<1477:CMEOTA>2.0.CO;2, 2002. 9347, 9353

**Ship-borne wind
profiling with lidar**

P. Achtert et al.

Title Page

Abstract

Introduction

Conclusions

References

Tables

Figures



Back

Close

Full Screen / Esc

Printer-friendly Version

Interactive Discussion

**Table 1.** System parameters of the HALO Doppler lidar.

| | |
|---------------------------|-------------------|
| Wavelength | 1.5 μm |
| Pulse repetition rate | 15 kHz |
| Sampling frequency | 50 MHz |
| Points per range gate | 6 |
| Number of pulses averaged | 30 000 |
| Averaging time | 2 s |
| Range resolution | 18 m |
| Focus | Infinity |

Ship-borne wind profiling with lidar

P. Achtert et al.

Table 2. Statistics of the linear fit between lidar and the sonic anemometer extrapolated to 75 m for different boundary layer depths (BLD).

| | BLD (m) | | | | | |
|-----------------------|---------|------|------|------|------|------|
| | 100 | 150 | 200 | 250 | 300 | 350 |
| <i>N</i> | 961 | 735 | 437 | 208 | 106 | 68 |
| Pearson's <i>r</i> | 0.92 | 0.92 | 0.93 | 0.92 | 0.91 | 0.89 |
| <i>R</i> ² | 0.85 | 0.84 | 0.86 | 0.85 | 0.82 | 0.80 |
| Intercept | 0.06 | 0.06 | 0.04 | 0.08 | 0.11 | 0.09 |
| Slope | 0.99 | 0.99 | 0.97 | 0.95 | 0.92 | 0.96 |

Title Page

Abstract

Introduction

Conclusions

References

Tables

Figures



Back

Close

Full Screen / Esc

Printer-friendly Version

Interactive Discussion



Ship-borne wind profiling with lidar

P. Achtert et al.

Table 3. Statistics of the linear fit between lidar and radiosounding as well as lidar and sonic anemometer on the bow mast. The lidar and radiosounding comparison has been conducted for a height of 75 m. The comparison of lidar and sonic anemometer has been performed for 75 m height with the sonic wind speed adjusted from 20 to 75 m following the method of Smith, 1988.

| | | Lidar vs. Radiosonde | | Lidar vs. Sonic anemometer |
|---------------------------|--------------------|----------------------|----------------|----------------------------|
| | | Wind speed | Wind direction | Wind speed |
| Geometrical wind solution | <i>N</i> | 175 | 163 | 637 |
| | Pearson's <i>r</i> | 0.92 | 0.98 | 0.91 |
| | R^2 | 0.85 | 0.96 | 0.81 |
| | Intercept | 0.71 | 4.35 | 1.00 |
| | Slope | 0.85 | 0.98 | 0.81 |
| Sinusoidal fit | <i>N</i> | 229 | 220 | 437 |
| | Pearson's <i>r</i> | 0.93 | 0.99 | 0.93 |
| | R^2 | 0.86 | 0.99 | 0.86 |
| | Intercept | 0.48 | 3.53 | 0.04 |
| | Slope | 0.89 | 0.98 | 0.97 |

[Title Page](#)
[Abstract](#)
[Introduction](#)
[Conclusions](#)
[References](#)
[Tables](#)
[Figures](#)
[Back](#)
[Close](#)
[Full Screen / Esc](#)
[Printer-friendly Version](#)
[Interactive Discussion](#)


Ship-borne wind
profiling with lidar

P. Achtert et al.

Title Page

Abstract

Introduction

Conclusions

References

Tables

Figures

◀

▶

◀

▶

Back

Close

Full Screen / Esc

Printer-friendly Version

Interactive Discussion



Table 4. Statistics of the linear fit between lidar and radiosounding at heights of 75, 100, 400, 600, and 700 m.

| | Wind Speed | | | | | | Wind Direction | | | | | |
|--------------------|------------|------|------|------|-------|------|----------------|------|-------|------|-------|--------|
| | 75 | 100 | 200 | 400 | 600 | 700 | 75 | 100 | 200 | 400 | 600 | 700 |
| Height (m) | 75 | 100 | 200 | 400 | 600 | 700 | 75 | 100 | 200 | 400 | 600 | 700 |
| <i>N</i> | 229 | 226 | 182 | 90 | 47 | 37 | 220 | 219 | 181 | 90 | 43 | 35 |
| Pearson's <i>r</i> | 0.93 | 0.94 | 0.97 | 0.97 | 0.98 | 0.98 | 0.99 | 0.99 | 0.99 | 0.99 | 0.99 | 0.99 |
| R^2 | 0.86 | 0.88 | 0.94 | 0.94 | 0.96 | 0.96 | 0.99 | 0.99 | 0.99 | 0.98 | 0.97 | 0.97 |
| Intercept | 0.48 | 0.64 | 0.45 | 0.14 | -0.48 | 0.15 | 3.53 | 5.12 | -0.46 | 0.43 | -5.78 | -12.95 |
| Slope | 0.89 | 0.96 | 1.00 | 1.01 | 1.06 | 1.03 | 0.98 | 0.93 | 0.99 | 1.00 | 1.01 | 1.03 |

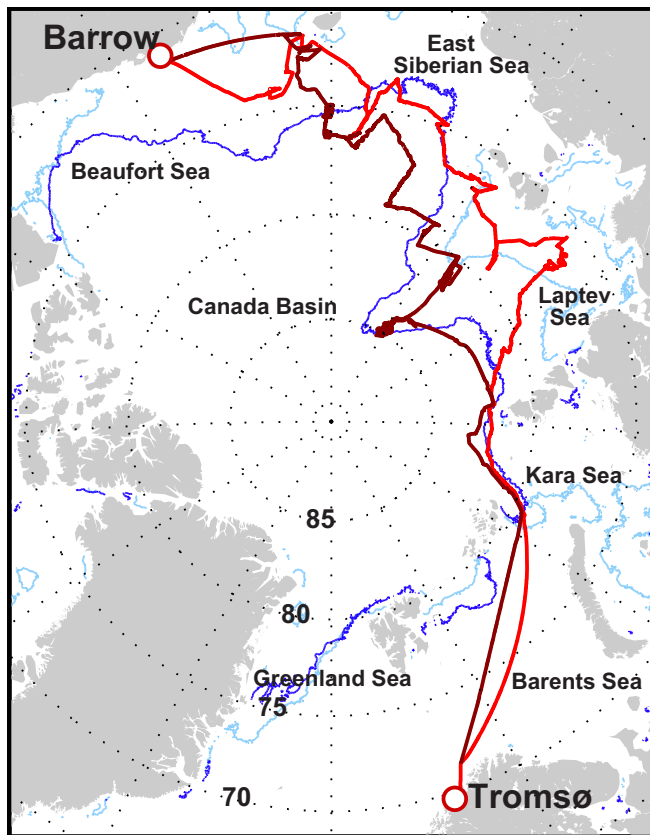


Figure 1. Cruise track of the legs from Tromsø to Barrow (red) and back (brown). Ice edges at the times of start and end of the cruise are shown in light and dark blue, respectively.

Ship-borne wind profiling with lidar

P. Achtert et al.

Title Page

Abstract

Introduction

Conclusions

References

Tables

Figures

◀

▶

◀

▶

Back

Close

Full Screen / Esc

Printer-friendly Version

Interactive Discussion



**Ship-borne wind
profiling with lidar**

P. Achtert et al.

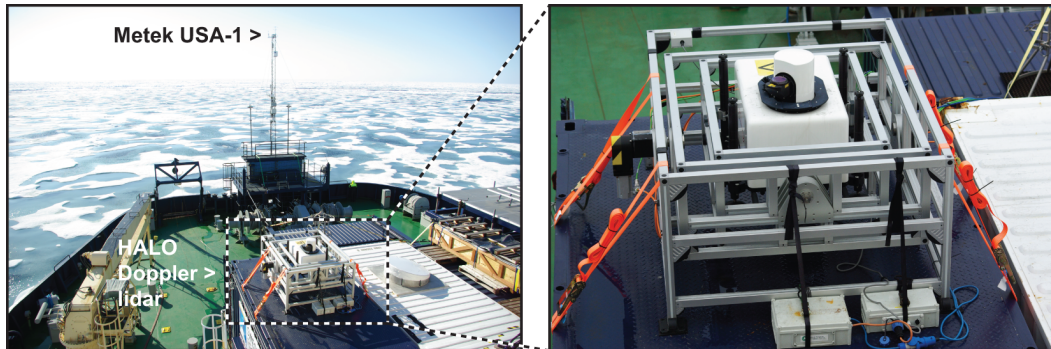


Figure 2. *Oden* foredeck (left) showing the lidar mounted within its motion-stabilised platform (right) and the Metek USA-1 sonic anemometer mounted on a mast over the bow of the ship.

[Title Page](#)[Abstract](#)[Introduction](#)[Conclusions](#)[References](#)[Tables](#)[Figures](#)[◀](#)[▶](#)[◀](#)[▶](#)[Back](#)[Close](#)[Full Screen / Esc](#)[Printer-friendly Version](#)[Interactive Discussion](#)

Ship-borne wind profiling with lidar

P. Achtert et al.

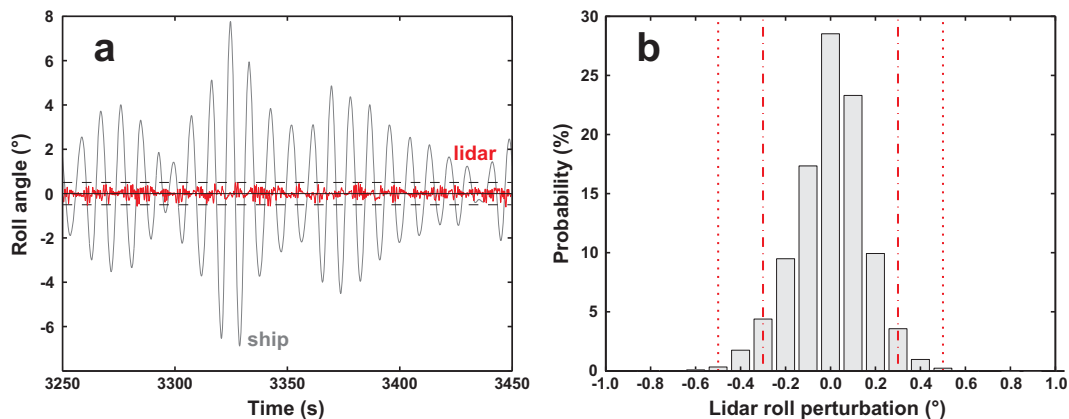


Figure 3. (a) Time series of ship and lidar roll angles on 18 September 2014 (05:54:10–05:57:30). Horizontal dashed lines indicate $\pm 0.5^\circ$. (b) Probability distribution of the lidar roll angle over the hour 05:00–06:00 on 18 September 2014. Red dotted lines indicate $\pm 0.5^\circ$, dot-dashed lines indicate $\pm 0.3^\circ$.

[Title Page](#)[Abstract](#)[Introduction](#)[Conclusions](#)[References](#)[Tables](#)[Figures](#)[◀](#)[▶](#)[◀](#)[▶](#)[Back](#)[Close](#)[Full Screen / Esc](#)[Printer-friendly Version](#)[Interactive Discussion](#)

Ship-borne wind profiling with lidar

P. Achtert et al.

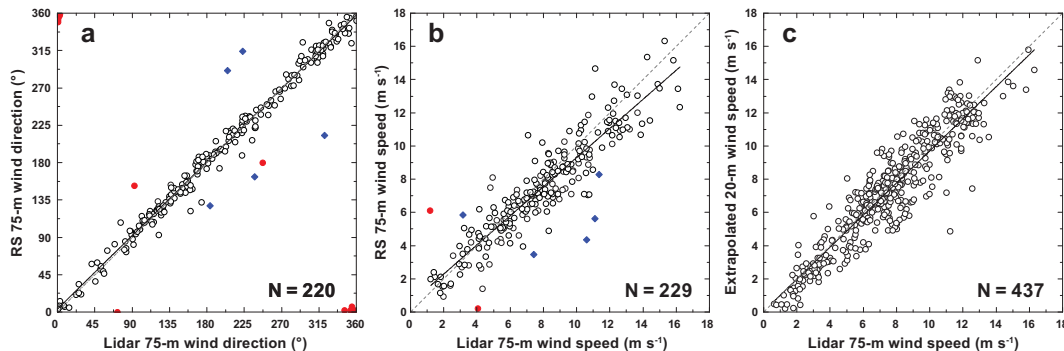


Figure 4. Doppler lidar evaluation: The sinusoidal fit solution is compared to data from radiosondes launched every 6 h from *Oden* (**a**, **b**) and the sonic anemometer on the bow mast (**c**). Number of points and linear fit parameters are given in Table 2; red points indicate outliers in wind direction. The blue diamonds (**a**, **b**) show comparison points obtained when the stabilization platform was turned off.

[Title Page](#)[Abstract](#)[Introduction](#)[Conclusions](#)[References](#)[Tables](#)[Figures](#)[⏪](#)[⏩](#)[◀](#)[▶](#)[Back](#)[Close](#)[Full Screen / Esc](#)[Printer-friendly Version](#)[Interactive Discussion](#)

Ship-borne wind profiling with lidar

P. Achtert et al.

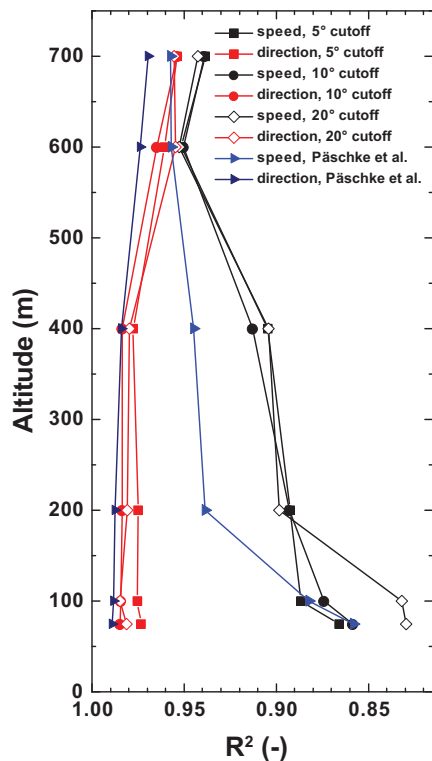


Figure 5. Squared correlation coefficient of derived wind speed (black) and wind direction (red) from lidar vs. radiosonde for different altitudes. Squares, circles and diamonds refer to cut-off angles of 5, 10 and 20° in the change of heading of the ship during one scan. Values for the intercept and slope for a cut-off angle of 10° are given in Table 4. The blue line refers to findings obtained using the quality assurance criteria of Päschrke et al. (2015).

Title Page

Abstract

Introduction

Conclusions

References

Tables

Figures

◀

▶

◀

▶

Back

Close

Full Screen / Esc

Printer-friendly Version

Interactive Discussion



Ship-borne wind profiling with lidar

P. Achtert et al.

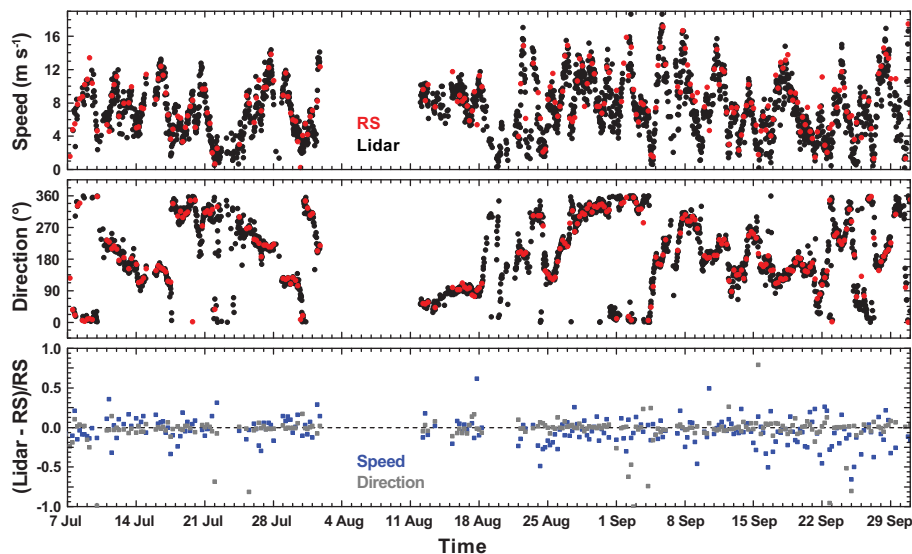


Figure 6. Time series of lidar (black) and radiosonde (red) wind speed (top) and wind direction (middle) at 100 m a.s.l. The bottom panel shows the relative difference normalised for wind speed (blue) and direction (gray).

[Title Page](#)[Abstract](#)[Introduction](#)[Conclusions](#)[References](#)[Tables](#)[Figures](#)[◀](#)[▶](#)[◀](#)[▶](#)[Back](#)[Close](#)[Full Screen / Esc](#)[Printer-friendly Version](#)[Interactive Discussion](#)

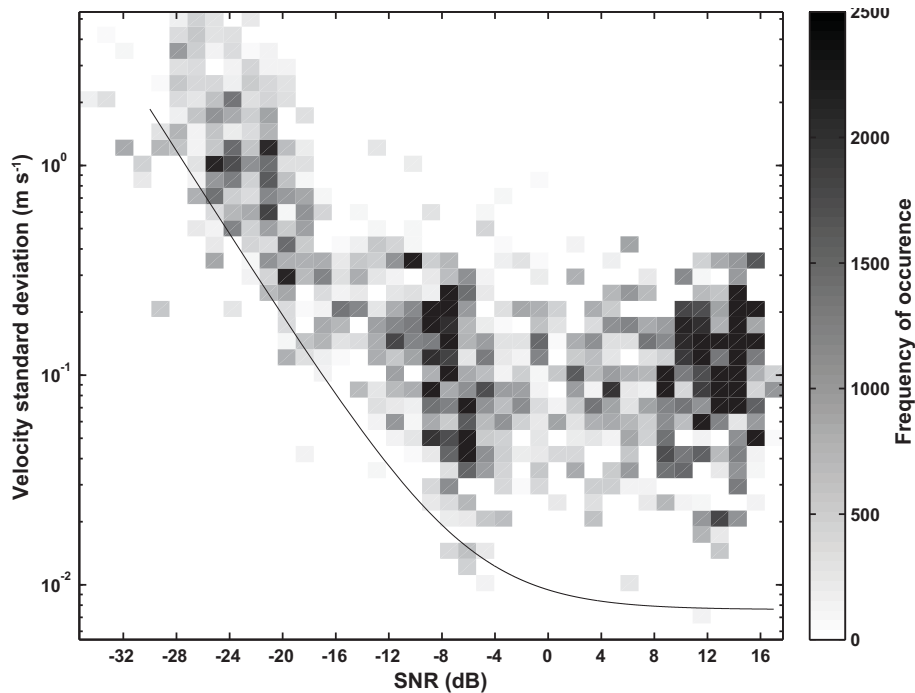


Figure 7. Standard deviations of the Doppler velocity determined from the zero leg impulse in the auto-covariance and the theoretical standard deviation (black line) for a signal spectral width of 2 m s^{-1} .

Ship-borne wind profiling with lidar

P. Achtert et al.

| | |
|--------------------------|--------------|
| Title Page | |
| Abstract | Introduction |
| Conclusions | References |
| Tables | Figures |
| ◀ | ▶ |
| ◀ | ▶ |
| Back | Close |
| Full Screen / Esc | |
| Printer-friendly Version | |
| Interactive Discussion | |



Ship-borne wind profiling with lidar

P. Achtert et al.

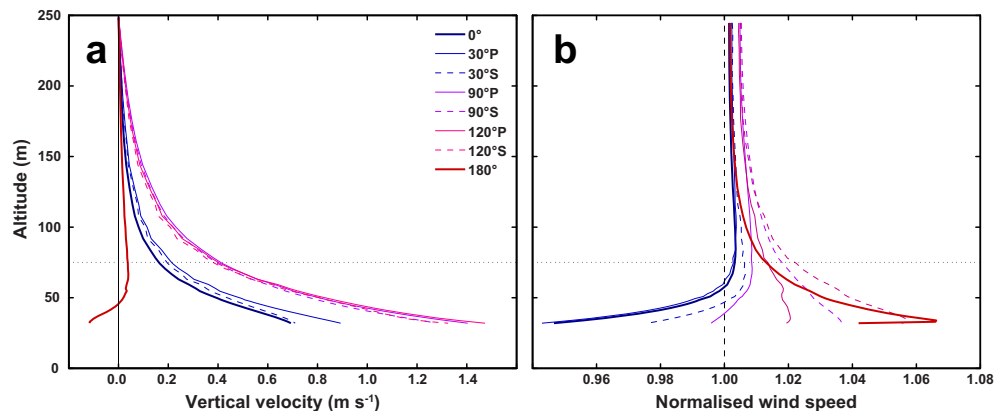


Figure 8. CFD study results above the shipboard lidar location: **(a)** profiles of vertical velocity above the lidar for various wind directions (port and starboard, relative to the bow). **(b)** Profiles of the horizontal wind speed, normalised by the free-stream profile for various wind directions (port and starboard) with respect to the bow. The horizontal dotted line indicates 75 m above the surface, the lowest level of reliable Doppler velocity measurements. Data is shown only for altitude > 31.5 m, the approximate level of the first lidar range gate.

[Title Page](#)[Abstract](#)[Introduction](#)[Conclusions](#)[References](#)[Tables](#)[Figures](#)[◀](#)[▶](#)[◀](#)[▶](#)[Back](#)[Close](#)[Full Screen / Esc](#)[Printer-friendly Version](#)[Interactive Discussion](#)